Optical tuning of silicon photonic structures with nematic liquid crystal claddings

Joanna Ptasinski,[1,2,*] Sung W. Kim,[1] Lin Pang,[1] Iam-Choon Khoo,[3] and Yeshaiahu Fainman[1]

[1]*Department of Electrical and Computer Engineering, University of California San Diego, La Jolla, California 92037, USA*

[2]*Space and Naval Warfare Systems Center Pacific, San Diego, California 92152, USA*

[3]*Electrical Engineering Department, Pennsylvania State University, University Park, Pennsylvania 16802, USA*

**Corresponding author: jptasins@ucsd.edu*

Received February 20, 2013; revised April 26, 2013; accepted May 9, 2013;
posted May 13, 2013 (Doc. ID 185555); published June 3, 2013

An analysis of and experimental demonstration of active optical tuning of silicon strip waveguides with methyl red doped nematic liquid crystal claddings is presented. Under low-power irradiation by polarized light, the reorientation of the nematic, the resulting index change, and phase shift produce a tuning range of 5.6 nm for the microresonator resonances. © 2013 Optical Society of America

OCIS codes: (130.2790) Guided waves; (130.3120) Integrated optics devices; (130.3130) Integrated optics materials; (160.3710) Liquid crystals; (160.5320) Photorefractive materials; (220.0220) Optical design and fabrication.
http://dx.doi.org/10.1364/OL.38.002008

Silicon photonics is a rapidly evolving field allowing for optical devices to be made inexpensively using standard semiconductor fabrication techniques and integrated with microelectronic chips. Optical circuits components that are tunable are clearly more desirable for developing compact, versatile, and agile devices [1,2]. Active tuning of modulators and ring resonator silicon photonic structures has been demonstrated using thermal, electrical, and optical means [3–5]. The underlying mechanisms include free-carrier injection through two-photon absorption using 10 ps pump pulses, photo-induced cladding refractive index change of an nm-fiber with a knot structure [4], or the refractive index of a material that is infiltrated inside a host silicon matrix [5].

In this work we present a chip-scale, CMOS-compatible, active optical tuning scheme for silicon devices achieving an experimental spectral shift of 5.6 nm for a ring resonator silicon structure with a nematic liquid crystal (NLC) cladding. NLCs are known for their extraordinary electro-optic sensitivity and broadband birefringence and are being exploited in many optoelectronic image display, sensing, and processing devices [6]. The liquid crystal (LC) reorientation, and therefore the birefringence change needed for tuning and switching purposes, usually employs an AC electric field [7–12]. Owing to their extraordinarily large optical nonlinearities, photomanipulation of NLC orientation has emerged as a promising alternative [13–18], due to their noncontact, electrode-free nature and the flexibility in the applied (optical) electric field directions. In the presence of small amounts (~1%) of light-absorbing Azo dyes, such as methyl red (MR), the reorientation effect is greatly amplified due to several mechanisms [17–22]. In our study, the main mechanism at work is attributed to the intramolecular torque exerted by the laser-excited Azo dye molecules on the LC director axis, resulting in reorientation of the LC director axis orthogonal to the light polarization direction; such mechanism underlies the extraordinarily large optical nonlinearities [20–22].

A schematic of our device is shown in Figs. 1(A) and 1(B). The silicon strip waveguides are surrounded by a lower-index LC cladding. This approach enables high modal confinement and small ring size. Typical metrics for silicon photonic ring filters include the center frequency, free spectral range (FSR), and the Q factor. The resonance width and FSR can be further used to calculate the finesse, which relates the internal and external losses of the resonator. LC properties pertinent to our experiment include birefringence, ac and optical dielectric anisotropies, and clearing temperature. For a feasibility demonstration, we chose 4-Cyano-4′-pentylbiphenyl (5CB) LC, which is a commonly used nematic; in the 1550 nm region $\Delta n = 0.158$ at room temperature.

To study the tuning of such 5CB cladded structures, 2D finite-element simulations were implemented in COMSOL Multiphysics. The effective index method was used in defining the effective mode indices and propagation constants for TE and TM modes of our ring resonator. Since TM modes are less confined to the core region, they are more susceptible to the LC birefringence effects. In practice, however, TE modes are preferred since TE is the ground mode of the waveguide and the strong modal confinement of TE polarized light enables sharp bends, thereby realizing dense photonic integrated circuits on a single silicon chip. Coupling to the device is

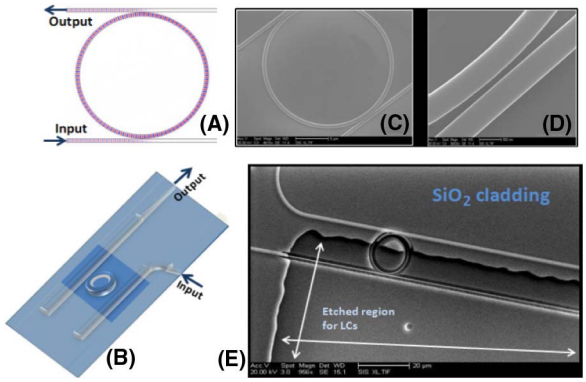

Fig. 1. (A) Simulated ring resonator structure showing critical coupling. (B) Schematic of the ring resonator device used in the experiment; window regions in the SiO_2 cladding allow room for LCs. (C)–(E) Fabricated devices; (E) shows the fabricated ring resonator with an etched region for LCs.

achieved by placing a bus waveguide adjacent to the ring at a distance, allowing for evanescent mode overlap. A resonance occurs when the optical path length of the resonator is exactly a whole number of wavelengths and the spacing between the resonances is referred to as the FSR [23]. The shift in the resonant wavelength takes place due to a change of the effective index of the resonant mode n_{eff} [23], given by

$$\Delta\lambda = \frac{L}{m}\Delta n_{\text{eff}(\lambda_1-\lambda_2)}, \tag{1}$$

where m indicates the order of the resonance, L is the circumference of the resonator, λ is the free-space wavelength of the resonant frequency, and $\lambda_1 - \lambda_2$ is the change in the resonant wavelength as a function of changing cladding index. Length of the device ring perimeter plays a significant role in the observable amount of resonant wavelength shift for a particular Δn_{eff}.

Our ring resonator devices consist of two 550 nm wide, 30 μm long waveguides separated by 100 nm from a centrally situated 19.8 μm diameter ring (also 550 nm wide). Tuning of the ring resonator depends on how far the mode extends into the cladding regions, the amount of space in the coupling region between the ring and waveguide, and the accrued losses (including coupling to bus waveguides), as well as the initial alignment of LCs. The silicon dioxide cladding region expands to cover a third of the ring in order to break the ring symmetry, as otherwise the effective index changes stemming from the contributions of the two linear polarizations may cancel each other, resulting in a null shift of the resonance. Our model showed that at room temperature, the ring resonator would sustain a resonance shift of 17.1 nm for TE modes in the case of maximum LC refractive index change of $\Delta n = 0.1584$, and a 5.7 nm shift when $\Delta n = 0.06$, as depicted in Fig. 2.

In our experimental studies, samples were fabricated using a silicon on insulator wafer composed of a 250 nm silicon layer positioned on top of 3 μm SiO_2 and with a silicon handle. The 3 μm buried oxide layer aids in preventing the evanescent field of the optical mode from

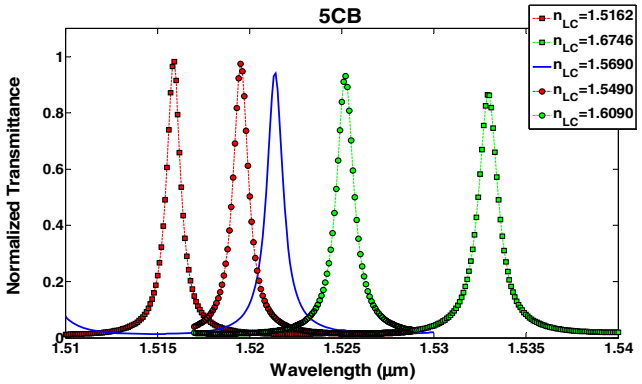

Fig. 2. Simulation result for TE modes of the ring resonator structure. Tuning of the resonance peak as a function of changing 5CB LC cladding index. The smooth line represents the resonance peak corresponding to n_i. The maximum shift in the resonance peak is 17.1 nm (square markers), while a $\Delta n = 0.06$ results in a resonance shift of $\Delta\lambda = 5.7$ nm (round markers).

penetrating the silicon substrate below. A 120 nm thick coat of hydrogen silsesquioxane resist spun on the wafer and patterned with electron beam lithography served as a mask for the dry etch of silicon. Samples were then exposed via JEOL JBX-5D11 system and dry etched using Oxford Plasmalab 100 RIE/ICP. The resulting silicon waveguides were covered by a 1.8 μm layer of SiO_2 cladding deposited via plasma-enhanced chemical vapor deposition. Window areas for LCs to break the ring symmetry were patterned with S1805 photoresist, exposed in an Hybrid Technology Group (HTG) Mask Aligner, and etched in a buffered oxide solution. The remaining S1805 photoresist was removed with acetone. The fabricated structures are depicted in Figs. 1(C)–1(E).

Linear inverse tapers were implemented to aid in low loss coupling from an optical fiber to the on-chip waveguide [24]. These adiabatically widened tapers work by increasing the mode size of the waveguide to that of the fiber. A polarizer in the output path allowed for a selection of TE transmission (horizontal polarization) or TM transmission (vertical polarization). Control of the telecom source, the power meter, and the source step size was automated.

A 470 nm Mightex LED source coupled with a polarizer and a quarter wave plate was focused onto the sample with a planoconvex lens. The wavelength of the source was chosen to coincide with the MR dye absorption spectrum. The quarter wave plate in conjunction with the polarizer allowed for linear or circular polarization of the LED source. The output power irradiating the sample was 85 μW with a spot size of 0.49 cm^2. It should be noted that the LC realignment depends on the UV source dosage (in our case the dosage was 0.2082 J/cm^2) and not on the intensity alone. The experimental setup is depicted in Fig. 3(A).

Nematic 5CB LCs mixed with MR dye at a 1% concentration of MR were used. A higher MR concentration provides for a larger effect and lower tuning optical power, but it also results in larger losses. A drop of

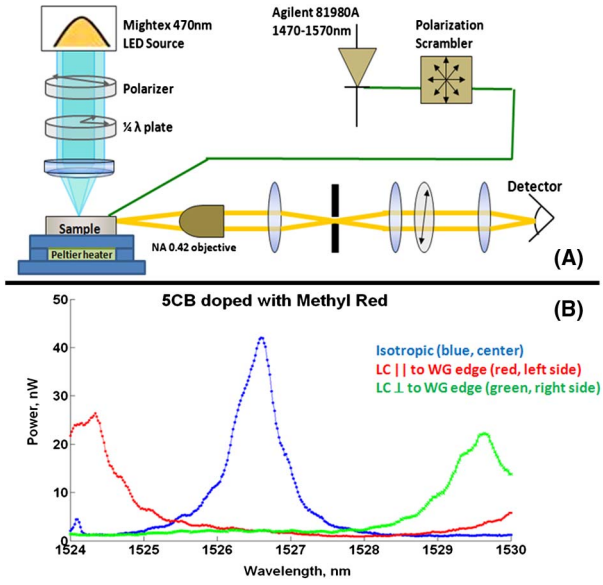

Fig. 3. (A) Experimental setup. (B) Experimental results of 5CB LC doped with MR dye.

LC material was placed onto the window regions of the sample and heated at 40°C (above isotropic temperature of 5CB) for 10 min in order for the LC material to completely fill the cell, then cooled back to room temperature and held at 24°C. Next, the 470 nm source was turned on, the quarter wave plate and linear polarizer were set to result in circular polarization, and linear polarizations and the corresponding measurements were made. It should be noted that the use of circular polarization at the beginning of the experiment causes the LC to be randomly oriented in addition to accounting for the average absorption that causes heating of the structure and a resulting resonance shift due to thermo-optic effects; in this sense, the measurement with circular polarization serves as a reference, while the linear polarizations then enable us to isolate LC reorientation from heating.

Our preliminary experimental results, appearing in Fig. 3(B), yield a 5.6 nm resonance shift; the location of the resonance was calculated using center of mass, which provides for higher accuracy as compared to tracking the peak value. This resonance shift agrees with the simulated result corresponding to $\Delta n = 0.06$. The effective LC index change is usually much smaller than the maximum, since LC molecules strongly anchored at the waveguide-cladding interface do not reorient from their initial alignment. We also note that the resonance peak in the measured result does not coincide with the simulated resonance peak. This difference arises due to fabrication errors in electron beam writing, pattern transfer, reactive ion etching, and wet etching steps [25], as well as some randomness in the initial LC surface alignment. The measured Q factor of our resonator is calculated as 2544, and our measured FSR = 8.5 nm, resulting in a finesse of 14.2. The Q factor and finesse of our device can further be improved by tuning the perimeter of the resonator and by increasing the distance between the bus waveguide and the ring, thus resulting in a smaller full width at half-maximum of the resonance.

In conclusion, we presented theoretically and experimentally the feasibility of low-power phototuning of silicon photonic structures with a dye-doped NLC cladding. The observed unoptimized resonance shift of 5.6 nm is in close agreement with the simulated result when $\Delta n = 0.06$. It can be further improved by other choices of dye dopants or LCs, surface alignment and anchoring conditions, and waveguide/resonator parameters. Optical tuning offers the advantage of noncontact, electrode-free, and configuration flexibility, and thus such optically tunable silicon photonic devices are likely to play an increasingly central role in all-optical circuit components and silicon photonic platforms.

This work was supported by the Defense Advanced Research Projects Agency, the Air Force Office of Scientific Research, the NSF Center for Integrated Access Networks, and SPAWAR Systems Center Pacific. We acknowledge useful discussions with Prof. Uzi Effron and thank Bill Mitchell (UCSB) for ebeam exposure.

References

1. J. Cos, J. Ferré-Borrull, J. Pallarès, and L. F. Marsal, Phys. Status Solidi C **8**, 1075 (2011).
2. A. W. Domanski, D. Budaszewski, M. Sierakowski, and T. R. Wolinski, Opto-Electron. Rev. **14**, 305 (2006).
3. V. R. Almeida, C. A. Barrios, R. R. Panepucci, and M. Lipson, Nature **431**, 1081 (2004).
4. Z. Chen, V. K. S. Hsiao, X. Li, Z. Li, J. Yu, and J. Zhang, Opt. Express **19**, 14217 (2011).
5. S. M. Weiss and P. M. Fauchet, Proc. SPIE **6017**, 60170H (2005).
6. I. C. Khoo and S. T. Wu, *Optics and Nonlinear Optics of Liquid Crystals* (World Scientific, 1995).
7. B. Maune, R. Lawson, G. Gunn, A. Scherer, and L. Dalton, Appl. Phys. Lett. **83**, 4689 (2003).
8. W. De Cort, J. Beeckman, R. James, F. A. Fernández, R. Baets, and K. Neyts, Opt. Lett. **34**, 2054 (2009).
9. A. T. Cai, Q. Liu, Y. Shi, P. Chen, and S. He, Appl. Phys. Lett. **97**, 121109 (2010).
10. W. De Cort, J. Beeckman, R. James, F. A. Fernandez, R. Baets, and K. Neyts, J. Opt. Soc. Am. B **28**, 79 (2011).
11. W. De Cort, J. Beeckman, T. Claes, K. Neyts, and R. Baets, Opt. Lett. **36**, 3876 (2011).
12. T. J. Wang, S. C. Yang, T. J. Chen, and B. Y. Chen, Opt. Express **20**, 15853 (2012).
13. I. C. Khoo, J. Opt. Soc. Am. B **28**, A45 (2011).
14. Y. H. Zhao, Q. Hao, Y. Ma, M. Q. Lu, B. X. Zhang, M. Lapsley, I. C. Khoo, and T. J. Huang, Appl. Phys. Lett. **100**, 053119 (2012).
15. I. C. Khoo, K. L. Hong, S. Zhao, D. Ma, and T. H. Lin, Opt. Express **21**, 4319 (2013).
16. U. A. Hrozhyk, S. V. Serak, N. V. Tabiryan, and T. J. Bunning, Adv. Mater. **19**, 3244 (2007).
17. C. T. Wang, H. C. Jau, and T. H. Lin, Opt. Lett. **37**, 2370 (2012).
18. I. C. Khoo, M. V. Wood, M. Y. Shih, and P. H. Chen, Opt. Express **4**, 432 (1999).
19. I. Janossy and L. Szabados, Phys. Rev. E **58**, 4598 (1998).
20. H. Zhang, S. Shiino, O. Tsutsumi, A. Kanazawa, T. Shiono, and T. Ikeda, Mol. Cryst. Liq. Cryst. **368**, 369 (2001).
21. I. C. Khoo, S. Slussarenko, B. D. Guenther, and W. V. Wood, Opt. Lett. **23**, 253 (1998).
22. W. M. Gibbons, P. J. Shannon, S. T. Sun, and B. J. Swetlin, Nature **351**, 49 (1991).
23. T. Baehr-Jones, M. Hochberg, C. Walker, E. Chan, D. Koshinz, W. Krug, and A. Scherer, J. Lightwave Technol. **23**, 4215 (2005).
24. G. Ren, S. Chen, Y. Cheng, and Y. Zhai, Opt. Commun. **284**, 4782 (2011).
25. H. Akhavan, M. El-Beheiry, and O. Levi, in *2012 International Symposium on Optomechatronic Technologies* (IEEE, 2012), pp. 1–4.